ELSEVIER

Applied Surface Science 141 (1999) 357–365

applied surface science

Surface roughness of thin layers—a comparison of XRR and SFM measurements

O. Filies [a], O. Böling [a], K. Grewer [a], J. Lekki [b,*], M. Lekka [b], Z. Stachura [b], B. Cleff [a]

[a] *Institute of Nuclear Physics, University of Münster, Münster, Germany*
[b] *Institute of Nuclear Physics, Radzikowskiego 152, 31-342 Cracow, Poland*

Received 29 May 1998; accepted 12 August 1998

Abstract

X-ray reflectivity (XRR) studies of thin layers (3 to 120 nm thick) were performed for the determination of layer thickness, density and roughness. The simulations of X-ray reflectivity measurements were performed using Parrat's recursive algorithm, while those of the reflection of X-rays from interfaces were performed using Fresnel formulae. Using this approach, the roughness of the interface was described by intensity damping by gaussian type functions. This allowed for the determination of layer thickness and density and average interface roughness. As an extension of this simple model, an enhanced theoretical description of rough interfaces proposed by Sinha was applied, where the X-ray reflection from interfaces was separated into a direct fraction and a diffuse scattered one with the use of the first Born approximation. A simulation procedure, calculating both fractions of the reflection was developed, that enabled the detailed characterisation of layers and inner layers. The complementary information required for proper adjusting of input simulation parameters was obtained from SFM measurements of the investigated surfaces. Surface roughness was described using fractal surface functions instead of simple gaussian peaks. A comparison between this method and SFM measurement shows a reasonable agreement, particularly in the estimation of shapes of interface structures.

PACS: 68.35Bs; 78.20Ci; 07.79

Keywords: X-ray reflectivity (XRR); SFM; Thin layers; Surface roughness; Fractal surface scaling

1. Theoretical background

X-ray reflectivity technique is a relatively simple, but powerful method for the determination of thin layer density, thickness and layer interface roughness. It allows also nondestructive studies of inner layers. Standard simulation methods of such X-ray spectra use a simple, but functional term for the description of the interface roughness in a form of X-ray intensity damping.

X-ray reflections from multilayer systems of $n-1$ layers and n interfaces may be calculated using Parrat's recursive formulae [1,2]. The idea of this approach is presented in Fig. 1.

* Corresponding author. Tel.: +48-12-637-0222 ext. 271; Fax: +48-12-637-1881; E-mail: lekki@alf.ifj.edu.pl

0169-4332/99/$ - see front matter
PII: S0169-4332(98)00524-8

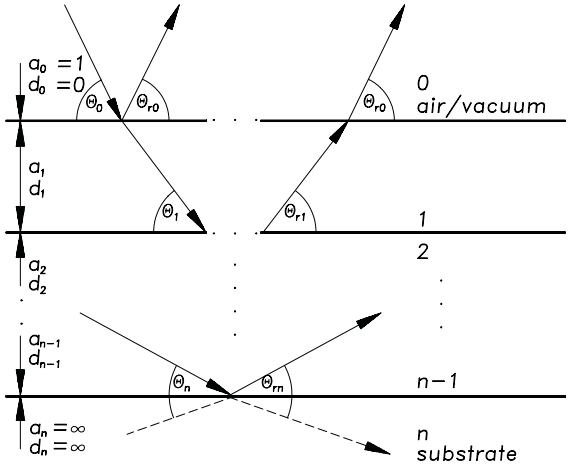

Fig. 1. The idea of the recursive approach: X-rays coming from medium 0 (air or vacuum) are scattered and deflected at the first interface (medium 1). The scattered fraction is again scattered and deflected at the next interface. This mechanism is reproduced until the last significant layer is reached. Every reflected fraction interferes with fractions reflected at previous interfaces, producing finally a measurable pattern.

For the ith interface the Fresnel factors f_i are defined by Eq. (1), while Fresnel coefficients F_{ij} (where $j = i + 1$) are calculated using Eq. (2).

$$f_i = \sqrt{\theta^2 - 2\delta_i - 2i\beta_i}\,, \tag{1}$$

where θ is an incident angle, δ is the dispersion factor and β represents absorption.

$$F_{ij} = \frac{n_i \sin\theta_i - n_j \sin\theta_j}{n_i \sin\theta_i + n_j \sin\theta_j} = \frac{f_i - f_j}{f_i + f_j}. \tag{2}$$

The distance d_n between interfaces (and therefore also the thickness of layer n) may be described using the exponential thickness factor a_n defined as follows:

$$a_n = \mathrm{e}^{-ik_1 f_n g_n/2} = \mathrm{e}^{(i\pi/\lambda) f_n d_n}, \tag{3}$$

where k_n is the wave vector in z-direction (perpendicular to the surface) and λ is the X-ray wavelength.

Therefore, the thickness factor a_n represents the attenuation of X-rays passing twice through layer n of thickness d_n. The thickness factor of medium 0 is neglected, i.e., $a_0 = 1$.

The final recursion formula constructed with the use of Eqs. (1)–(3) has the form:

$$R_{n-1,n} = a_{n-1}^4 \frac{R_{n,n+1} + F_{n-1,n}}{R_{n,n+1} F_{n-1,n} + 1}, \tag{4}$$

where:

$$F_{n-1,n} = \frac{f_n - f_{n-1}}{f_n + f_{n-1}}, \tag{5}$$

The X-ray reflection calculations should be started at the lowest significant layer n (i.e., for the layer number $n+1$ the factor $R_{n+1} = 0$ and $a_{n+1} = \infty$) and performed upwards until the topmost layer is reached.

2. Interface roughness—Névot's model

The simple model presented above describes only ideal interfaces: flat, homogeneous and isotropic. In real measurements, such conditions are not met: in general, the real surfaces are rough, inhomogeneous and anisotropic, while the most significant role is played by interface roughness.

The first simple description of interface roughness was presented by Névot et al. [3], where Gaussian functions were used for roughness modeling. According to their model, the rough interface may be approximated by a gaussian distribution of peaks and valleys with respect to the mean surface (Fig. 2).

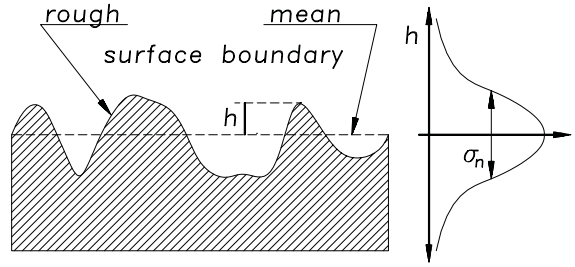

Fig. 2. Interface roughness according to Névot. The distribution of peaks and valleys on a mean interface level is described using the gaussian function and its σ parameter.

Thus, the roughness coefficient may be calculated [3] as:

$$\zeta_n = \exp\left(-8\pi\frac{\sigma_n^2}{\lambda^2} f_n f_{n-1}\right), \quad (6)$$

and the recursion from Eq. (4) should be corrected [4] to the form:

$$R'_{n-1,n} = R_{n-1,n}\zeta_n. \quad (7)$$

3. Fractal approach—Sinha's model

The simulation of real interfaces with the use of roughness coefficients ζ_n is only a rough approximation. Its weakness is particularly significant for non-gaussian type of roughness, for example, for surfaces with steps, periodical changes, etc. [5]. The simple model does not include the diffuse scattering from a rough surface, which may be significant. The model proposed by Sinha [6,7] and Palasantzas [8] brings a vast improvement of the simple model by separating the reflected X-ray beam into two fractions: specular and diffuse:

$$R = R_{\text{spec}} + R_{\text{diff}}. \quad (8)$$

The specular part corresponds to Fresnel equations for smooth surface, while the roughness influencing the diffuse fraction is described by a separate equation and treated as perturbation.

As a calculation tool serves the Born approximation (for large reflection angles) or Distorted Wave Born Approximation (DWBA, for small angles). In this way, it becomes possible to introduce into the theoretical model the interfaces described by growth functions (obtained, for example, by simulations of molecular beam epitaxy processes) or by dedicated interface functions used in the Kardar–Parisi–Zhang model [9,10]. In particular, it is possible to apply periodical [5,7] or fractal functions [11,12]. Fractal type surfaces may be characterized by their scaling property. Surface $z(r)$ is considered to be self-affine if the following simple equation is fulfilled:

$$\sigma(L) \sim L^h, \quad (9)$$

where L represents the length scale (system size) and σ is a well-known root-mean-square value of the surface height variable $\sigma^2 = \langle z^2(r)\rangle$. The Hurst exponent h $(0 \le h \le 1)$ contains information about the type of surface: low h values represent sharply formed surfaces, while higher h values correspond to mild curvatures.

Self-affine property may be introduced into X-ray reflectivity formulas through the definition of the mean-square height-deviation function $G(R)$:

$$G(R) = \langle [z(r) - z(r+R)]^2 \rangle, \quad (10)$$

closely related to a height–height correlation function $C(R)$:

$$C(R) = \langle [z(r) \times z(r+R)] \rangle, \quad (11)$$

by:

$$G(R) = 2[\sigma^2 - C(R)]. \quad (12)$$

In reality, for large separations $R \to \infty$, it is desirable to introduce the physical distance limitation, the

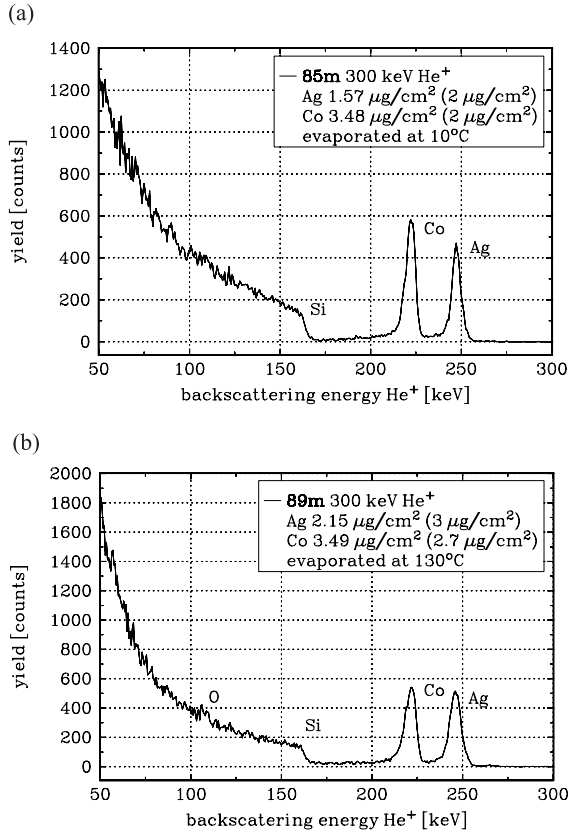

Fig. 3. TOF-RBS spectra of Co/Ag thin layers deposited on a Si substrate at 10°C (left) and 130°C (right). The measured mass density values are shown in figure insets (numbers in parentheses represent values expected from deposition conditions).

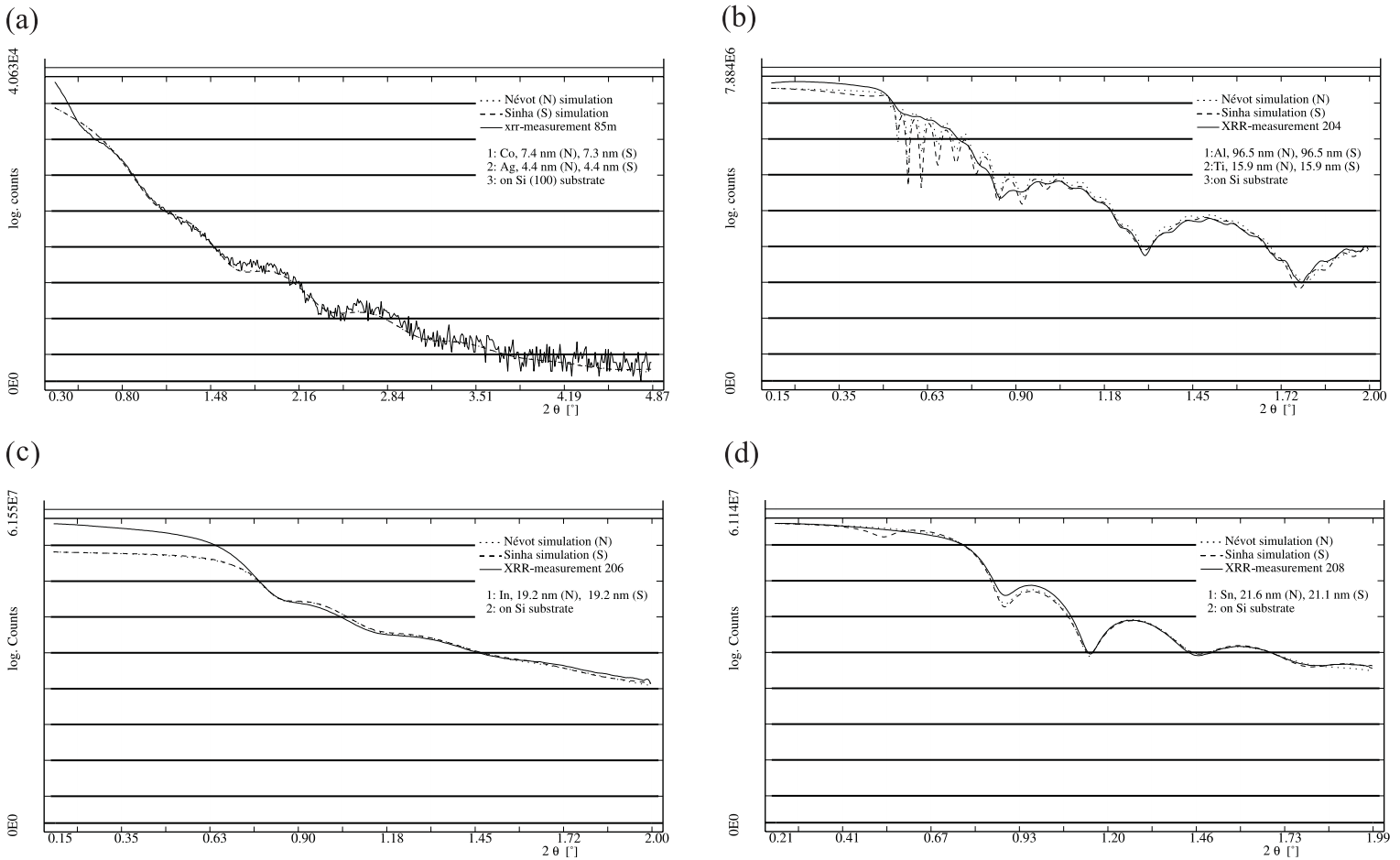

Fig. 4. XRR spectra and simulations performed according to Névot's and Sinha's algorithms for the following layers deposited on a Si substrate: (a) 7.3 nm Co/4.4 nm Ag double layer (Table 1, sample 1), (b) 96 nm Al/16 nm Ti double layer (sample 9), (c) 19 nm single In layer (sample 5), (d) 21 nm single Sn layer (sample 8). Layers' thickness were obtained from simulation following either Névot's or Sinha's model.

Table 1
The comparison of roughness parameters obtained for several selected samples from XRR and SFM measurements

Sample	Layer	Thickness (nm)	Roughness (nm) (N = Névot, S = Sinha)	Roughness (nm) (SFM)
1. Co/Ag on Si, evaporation at 10°C	Co	7.4 ± 0.7	0.29 ± 0.04 (NS)	2.06 ± 0.4
	Ag	4.44 ± 0.4	2.11 ± 0.32 (NS)	
	Si	–	0.85 ± 0.13 (NS)	
2. Co/Ag on Si, evaporation at 10°C	Co	8.1 ± 0.8	0.33 ± 0.05 (NS)	2.57 ± 0.5
	Ag	4.98 ± 0.5	2.01 ± 0.30 (NS)	
	Si	–	0.93 ± 0.14 (NS)	
3. Co/Ag on Si, evaporation at 130°C	Co	4.2 ± 0.4	1.36 ± 0.20 (S)	1.67 ± 0.6
	Ag	3.96 ± 0.4	0.30 ± 0.05 (S)	
	Si	–	0.5 ± 0.07 (S)	
4. Al_2O_3/Sn on Si, magnetron sputtering	Al_2O_3	99.4 ± 14.9	2.79 ± 0.56 (S)	3.71 ± 0.74
	Sn	19.9 ± 3.0	2.63 ± 0.53 (S)	
	Si	–	1.19 ± 0.24 (S)	
5. In on Si, magnetron sputtering	In	19.2 ± 1.9	0.79 ± 0.12 (S)	3.91 ± 0.78
	Si	–	2.29 ± 0.34 (S)	
6. Al_2O_3 on Si, magnetron sputtering	Al_2O_3	16.4 ± 1.6	1.17 ± 0.18 (N)	1.32 ± 0.27
	Si	–	0.71 ± 0.11 (N)	
7. Ti on Si, magnetron sputtering	Ti	17.1 ± 1.7	1.40 ± 0.21 (S)	1.88 ± 0.38
	Si	–	0.47 ± 0.07 (S)	
8. Sn on Si, magnetron sputtering	Sn	21.06 ± 2.1	2.63 ± 0.53 (S)	1.93 ± 0.39
	Si	–	1.38 ± 0.28 (S)	
9. Al/Ti on Si, magnetron sputtering	Al	96.5 ± 14.5	2.54 ± 0.5 (NS)	35 ± 3 (!)
	Ti	15.8 ± 2.4	0.75 ± 0.15 (NS)	
	Si	–	1.04 ± 0.21 (NS)	

Layer thickness values were calculated from the XRR data analysis.

cutoff length ξ. In the simplest model, $G(R)$ and $C(R)$ functions may be represented by:

$$g(R) = 2\sigma^2\left[1 - \exp\left(-\left(\frac{R}{\xi}\right)^{2h}\right)\right],$$

$$C(R) = \sigma^2 \exp\left(-\left(\frac{R}{\xi}\right)^{2h}\right), \qquad (13)$$

Then, using the previously mentioned mixture of the Born approximation and DWBA, the reflection described by Eq. (7) should be modified to the form:

$$R'_{n,n-1} \cong R_{n,n-1}\zeta_{n,n-1} + R_{n,n-1}\zeta_{n,n-1}(1 - F_{n,n-1})^2 \times \int \left(\exp\left(f_n^2 C(R)\right) - 1\right) J_0(R)\, R\, \mathrm{d}R, \qquad (14)$$

where $J_0(R)$ is the Bessel function and integration is performed over the full sample area. Eq. (14) was used as the computational basis for the X-ray reflectivity simulation and analysis software, DiffTool [13]. [1] The examples of its application are presented in the experimental part of the actual paper. The height–height correlation function $C(R)$ or mean-square height-deviation function $G(R)$ may be obtained from complementary measurements, and applied to X-ray reflectivity calculations. The most straightforward method for this purpose seems to be

[1] DiffTool is a complete application software for X-ray reflection (XRR) analysis and simulation, with the use of different simulation algorithms. The package contains also the correction and analysis tools for X-ray diffraction (XRD), small angle diffraction and rocking curve scans. DiffTool 1.01beta is freeware and can be downloaded from http://pikp15.uni-muenster.de/.

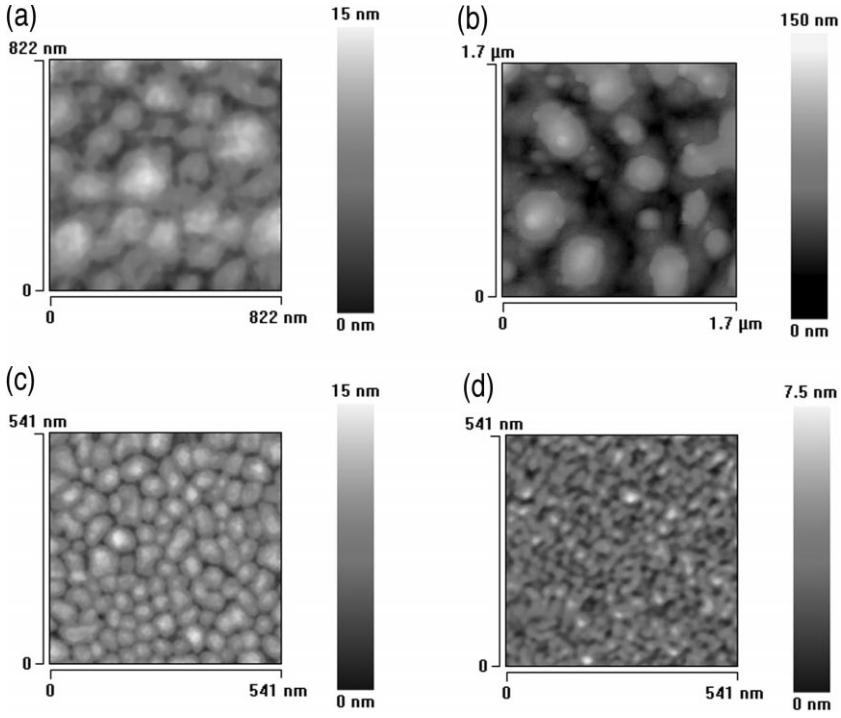

Fig. 5. Topography of four samples presented in Fig. 4 measured using SFM in air.

the scanning force microscopy (SFM), providing the real, three-dimensional topographical data. In this way both, $C(R)$ and/or $G(R)$ functions may be computed directly from the SFM data. The calculated functions may serve as a check of X-ray spectra simulation correctness and as a source of independently measured input values for the simulation procedure. Similar comparison was performed in a recently published work of Wang [14].

4. Experimental

The above approach was used for the characterization of several tens of metal and metal oxide layers, deposited on silicon substrates with the use of physical vapor deposition (PVD) and magnetron sputtering techniques. In order to assure diversified deposition conditions, deposition was performed at different temperatures, ranging from 10 to 130°C. Full results of all measurements and analyses are presented in Ref. [4]. In the present paper, several example cases will be presented.

Most of the samples were characterized by the time-of-flight Rutherford backscattering technique (TOF-RBS) using 300 keV He^+ ions. The RBS technique provided independent measurements of layers mass density (in $\mu g/cm^2$) and profile. Fig. 3 shows the TOF-RBS spectra of two double layer cobalt/silver structures evaporated on silicon substrate: the first one evaporated at 10°C and the second one at 130°C. Both measurements yield quite close values of cobalt and silver mass densities. Fig. 4 presents XRR measurements (logarithm of counts vs. detection angle) and simulations performed using Névot's and Sinha's algorithms of four selected samples.

XRR spectra deliver more information than the TOF-RBS measurements: from simulations it is possible to gain both the layer thickness and the interface roughness, as is presented in Table 1. It is desirable however, that simulation should be justified using complementary measurements. Therefore, as the next step of experimental procedure, the SFM images of the same samples were collected (Fig. 5), using a home built scanning force microscope [15].

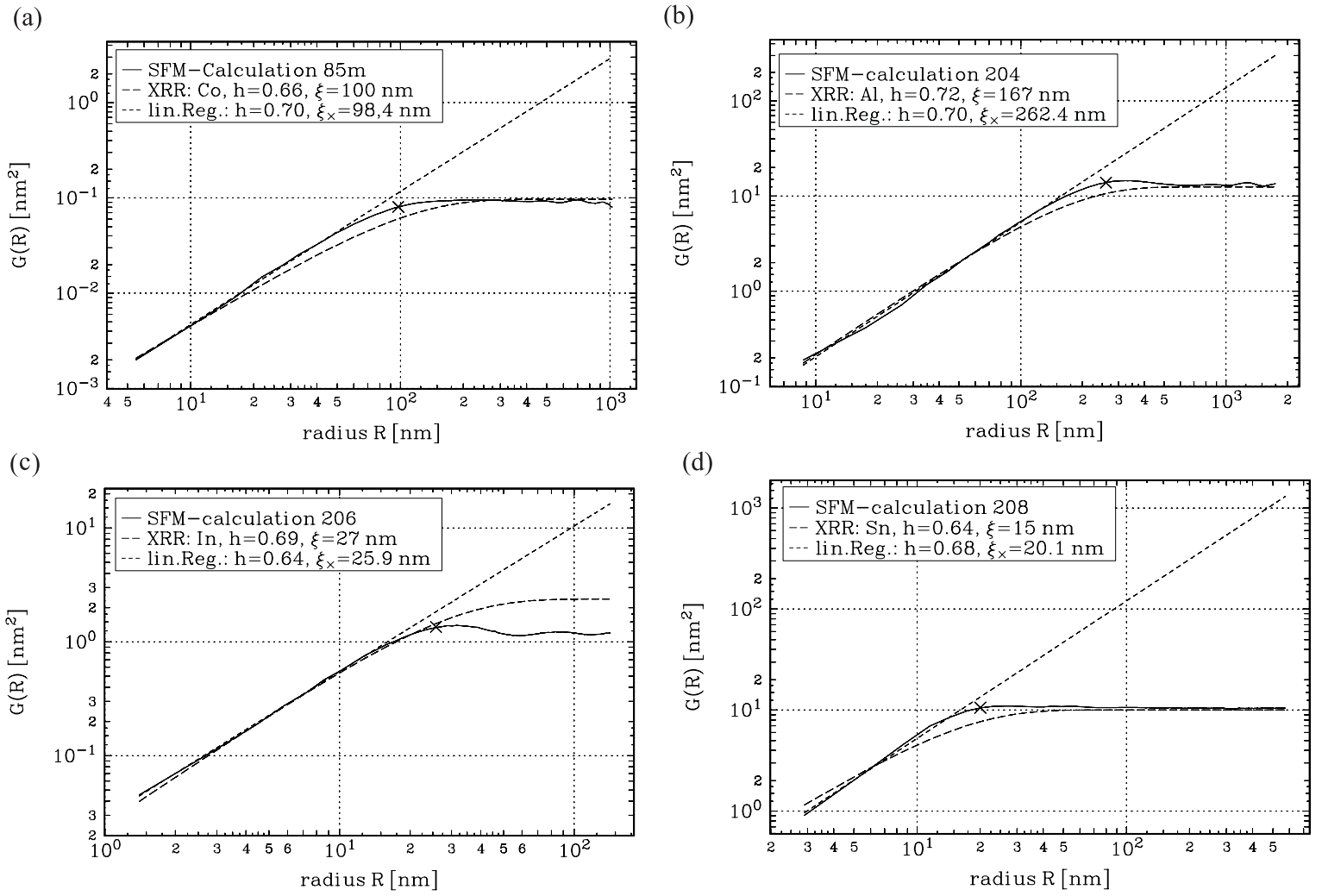

Fig. 6. A comparison of surface fractal scaling properties of four example surfaces (Figs. 4 and 5) measured using SFM (directly) and XRR (simulation according to Sinha's model).

All SFM data were obtained in air. The surfaces of samples show quite different character, depending not only on layer composition but also on deposition conditions.

Table 1 presents several comparisons between the root-mean-square surface roughness obtained from XRR spectra fitting and from SFM measurements. Both methods produce usually roughness values of the same range, where XRR data are usually smaller. Very often, for double layers with a relatively thin topmost layer (not exceeding 5–10 nm), estimated by XRR as very smooth, the SFM roughness corresponds to XRR simulation for the second, more rough layer. In several cases one can notice, however, that the SFM results are significantly higher than the corresponding XRR data (cf. position 9 in Table 1). This situation occurs always when a relatively flat surface is covered with more or less prominent islands (cf. Fig. 5b corresponding to position 9). In such case, X-rays are partially reflected from the surface (islands base) and partially from the islands upper regions (flat peaks), just like in case of existence of an additional thin layer, corresponding to peaks area. As a result, the surface roughness determined by XRR method is significantly diminished. This effect influences the range of applicability of XRR technique for surface roughness determination.

As it was shown in Eqs. (13) and (14), using XRR simulations performed according to Sinha's model and three dimensional topographic data obtained by SFM, it is possible to compare directly the fractal scaling properties of the surface studied by both methods. Fig. 6 shows a comparison of $G(R)$ function calculated from XRR and SFM data.

It is convenient to display the $G(R)$ function in a log–log scale. Then, the linear part of the plot represents the region of applicability of the surface scaling property (it is also the mean lateral structure size as illustrated in Fig. 5) and the linear slope is the measure of the Hurst exponent h. At some distances, linearity breaks down and the $G(R)$ function reaches slowly saturation. This length is a measure of the cutoff distance ξ and gives an estimate of the mean lateral extension of the surface structures.

In the case of SFM measurements it is possible to compute the $G(R)$ directly, according to Eq. (12). Then, the cutoff distance ξ and the Hurst exponent h may be obtained by simple fitting. For XRR measurements the definition of the $G(R)$ function from Eq. (13) must be used and the values of ξ and h are a result of fitting the XRR spectrum by Eq. (14).

$$\underbrace{\langle [z(\mathbf{r}) - z(\mathbf{r}+\mathbf{R})]^2 \rangle}_{\text{SFM, direct calculation}\uparrow} \equiv G(\mathbf{R}) = \underbrace{2\,[\sigma^2 - C(\mathbf{R})]}_{\uparrow\ \text{XRR, simulation}} \tag{15}$$

However, a reasonable agreement between SFM and XRR results was obtained in almost all cases, independent of deposition method and conditions. One can also notice that the range of mean lateral distance between the surface structures observed in SFM images corresponds to the cutoff distance ξ.

5. Conclusion

XRR and SFM measurements may be performed nondestructively in a very short time ($\sim$ 5 min) and do not require any special sample preparation. By obtaining surface roughness and scaling parameters from SFM measurements and applying them to simulations using the models of Névot and Sinha, it is possible to determine the following properties of layers and their interfaces:

- The average layer thickness for single- and multi-layer systems, taking into account sample porosity (which influences the simulation through lowering the film density). The range of applicability covers thicknesses from single nanometers to 200 nm, while the resolution of the fitting procedure is not worse than 10%. Best fits are obtained in the range of 10–100 nm.
- The average global interface roughness may be obtained, also for inner interfaces and buried layers. However, as the interface roughness influences strongly the interference conditions, it should not exceed the limit of $\sim$ 10 nm.

References

[1] L.G. Parrat, Phys. Rev. 95 (1954) 359–369.
[2] C. Rhan et al., J. Appl. Phys. 74 (1) (1993) 146–152.
[3] L. Névot et al., Rev. Phys. Appl. 15 (1980) 761–779.
[4] O. Filies, Röntgenreflektometrie zur Analyse von Dünnschichtsystemen-Charakterisierung ultradünner

Schichten, PhD thesis, Part I, Institute of Nuclear Physics, Münster, 1997.
[5] P. Doig et al., J. Appl. Cryst. 14 (1981) 321–325.
[6] S.K. Sinha, Acta Phys. Pol. A 89 (2) (1996) 219–234.
[7] S.K. Sinha et al., Phys. Rev. B 38 (4) (1988) 2297–2311.
[8] G. Palasantzas, Phys. Rev. E 49 (2) (1994) 1740–1742.
[9] M. Kardar et al., Phys. Rev. Lett. 56 (1986) 889–892.
[10] G. Palasantzas et al., Phys. Rev. B 48 (5) (1993) 2873–2877.
[11] A.-L. Barabasi, H.E. Stanley, Fractal Concepts in Surface Growth, Cambridge University Press, 1995.
[12] A. Bunde, S. Havlin, Fractals in Science, Springer-Verlag, 1995.
[13] O. Filies, DiffTool—Program zur Analyse von Röntgenspektren, PhD thesis, Part II, Institute of Nuclear Physics, Münster, 1997.
[14] J. Wang, Europhys. Lett. 42 (3) (1998) 283–288.
[15] J. Lekki, Scanning Force Microscopy of Implanted Silicon, PhD thesis, Institute of Nuclear Physics, Cracow, 1996.